Tight Integration of Feature-based Relocalization in Monocular Direct Visual Odometry

Mariia Gladkova[1,2], Rui Wang[1,2], Niclas Zeller[1,2], and Daniel Cremers[1,2]

Abstract— In this paper we propose a framework for integrating map-based relocalization into online direct visual odometry. To achieve map-based relocalization for direct methods, we integrate image features into Direct Sparse Odometry (DSO) and rely on feature matching to associate online visual odometry (VO) with a previously built map. The integration of the relocalization poses is threefold. Firstly, they are incorporated as pose priors in the direct image alignment of the front-end tracking. Secondly, they are tightly integrated into the back-end bundle adjustment. Thirdly, an online fusion module is further proposed to combine relative VO poses and global relocalization poses in a pose graph to estimate keyframe-wise smooth and globally accurate poses. We evaluate our method on two multi-weather datasets showing the benefits of integrating different handcrafted and learned features and demonstrating promising improvements on camera tracking accuracy.

Index Terms— SLAM, relocalization, map-based localization

I. INTRODUCTION

Visual odometry (VO) and visual Simultaneous Localization and Mapping (SLAM) are important components of many autonomous systems that use cameras as one of their sensor modalities. For these systems, detection of a re-visited place can be crucial in correcting accumulated drift [1], recovering from a tracking failure or solving the kidnapped robot problem [2]. These issues can be solved by camera-based *relocalization*, which in this work is referred to as a process of continuous online estimation of 6DoF poses based on a pre-generated map. We aim to extend the conventional use of relocalization as a recovery module [3], [4] and integrate its continuous estimates into a visual odometry (VO) framework in a much more involved fashion.

Relocalization is a challenging task, since appearance of a map sequence can differ significantly from the currently acquired visual data due to weather and seasonal changes as well as human activities like traffic and construction. While feature-based VO and SLAM methods can tackle this problem by relying on the repeatability and descriptiveness of local features, there is no straightforward way for direct methods to achieve relocalization. Usually direct methods sample points that hold only pixel intensity values, which cannot offer any of the aforementioned feature properties. Only limited efforts have been made to resolve such issue. In GN-Net [5], the raw images are replaced by learned feature maps to enhance the invariance to brightness changes. LDSO [6], on the other hand, proposes to integrate image
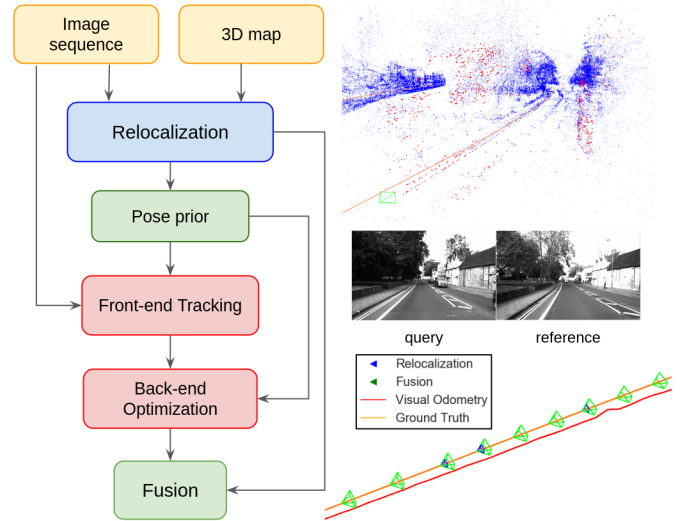
Fig. 1: Left: Proposed relocalization pipeline. The relocalization module estimates global camera poses against a pre-built map. Relocalization poses are tightly integrated into the front-end tracking and the back-end optimization of a direct VO framework to increase accuracy and robustness of camera pose estimation. Furthermore, the relative VO poses and global relocalization poses are fused in a pose graph optimization to obtain smooth and globally accurate poses. Top right: Overlay of the reference map (blue) with the VO point cloud (red). Bottom right: The fused poses (green) closely follow the ground truth trajectory (orange line).

features into DSO [7], thus combining the advantages of both families. In this work, we proceed in the direction of merging image features into direct methods. When a new frame arrives, in addition to tracking features with respect to a previous reference frame, we also track them against a pre-built map and obtain a relocalization pose by feature matching. We further propose to utilize relocalization poses at three levels: by incorporating them as pose priors in the front-end tracking, by tightly integrating them into the back-end bundle adjustment (BA), and by fusing the global relocalization poses with relative VO estimates to get a smooth and globally accurate trajectory. Tight integration of pose priors into a direct sparse odometry framework is inspired by the D3VO work [8], where relative camera transformations estimated by a deep network are utilized instead. To our knowledge our work is the first approach that introduces online relocalization for direct VO and tightly integrates the relocalization poses into the VO optimization

back-end. Along with our pose graph, optimization-based fusion we offer a complete direct visual SLAM system that provides globally and locally accurate camera localization in a monocular setting. Moreover, unlike LDSO [6] which considers only ORB features [9] for place recognition, feature tracking and matching, we integrate different handcrafted and learned features to unveil their pros and cons.

II. RELATED WORK

A. Indirect versus Direct VO / SLAM

Indirect VO / SLAM methods [10], [3], [4] have dominated the field for many years. Their success can be partially attributed to robust feature detectors and descriptors that incorporate invariance to geometric noise, brightness and viewpoint. An alternative, direct formulation, which skips abstraction into a feature space and directly works with pixel intensities, has been firstly proposed in [11] using an Extended Kalman Filter and was re-formulated as a non-linear optimization problem in [12], [7]. Direct methods sample interest points across an entire image space including edges and less-textured surfaces, which makes them generally more robust in cornerless environments. On the other hand, direct approaches are fragile to rapid motion and changes in illumination. Moreover, a good initialization is important to ensure optimization convergence and to guarantee an optimal solution. This makes direct methods inferior in wide-baseline matching, such as loop closure and relocalization, where global accuracy is desired. This issue is addressed in LDSO [6], where loop closures are achieved by adapting a point selection strategy and by introducing local features into a direct method.

B. Handcrafted and Learned Features

In recent years, the number of computer vision tasks that require feature matching has significantly increased [13], [14], [3], [15]. These applications introduce different feature requirements such as computational efficiency, invariance to scale and affine transformation, as well as robustness to noise and changes in lighting conditions. For many years SIFT [16] has been one of the most widely used feature descriptor, however its extraction is admitted to be computationally demanding [9]. Binary ORB features [9] that combine a FAST keypoint detector [17] and a BRIEF descriptor [18] have been proposed as an open-source, fast and lightweight alternative to SIFT. With the recent advances of deep learning, learned feature representations have shown a superior performance to handcrafted features [19]. Neural networks have been applied to separate tasks of keypoint localization [20], [21], descriptor learning [22], as well as to end-to-end feature extraction from images [23], [24]. In our work, we select three representative learned features, namely, SuperPoint [25], R2D2 [24] and ASLFeat [26]. They are integrated into a direct VO method and used to achieve map-based relocalization.

III. SYSTEM OVERVIEW

In the following sections we will describe in detail the proposed SLAM and relocalization framework as shown in Fig. 1. Our pipeline consists of three major modules: 1) a relocalization module that obtains reference poses with respect to a pre-build map (Sec. V); 2) a VO module that integrates the relocalization information to perform robust and accurate camera tracking within a local coordinate frame (Sec. IV); 3) a fusion module that fuses global map-based relocalization poses and relative visual odometry poses to obtain a smooth and globally accurate camera trajectory (Sec. VI). While our VO module uses information from the relocalization module, it is also used to generate the map we localize against. We will first describe our VO approach and afterwards proceed with the relocalization module. Finally, we will explain how both components are integrated in the fusion module.

IV. VISUAL ODOMETRY

Our VO module builds on top of DSO [7], a state-of-the-art direct visual odometry algorithm. For each new frame DSO estimates its initial pose with respect to a reference keyframe by direct image alignment. Poses of keyframes are then refined in a sliding window, where bundle adjustment jointly optimizes the depth of points and all keyframe poses by minimizing a photometric energy function

$$E_{\text{photo}} = \sum_{i \in \mathcal{F}} \sum_{\mathbf{p} \in \mathcal{P}_i} \sum_{j \in obs(\mathbf{p})} E_{\mathbf{p}j}, \quad (1)$$

where $\mathcal{F}$ is a set of all keyframes, $\mathcal{P}_i$ a set of points hosted in a keyframe i, and $obs(\mathbf{p})$ a set of keyframes that observe a point $\mathbf{p}$. $E_{\mathbf{p}j}$ is a weighted photometric error term for a point $\mathbf{p}$ hosted in a frame i and observed in a frame j. For details on the energy formulation please refer to [7].

A. Pose Priors

To improve the accuracy and robustness of VO, we use the information gained from relocalization against a pre-built map (Sec. V). The relocalization poses are used as priors for both the front-end tracking (coarse tracker) and the back-end bundle adjustment.

1) Pose Prior for Coarse Tracker: In the tracking front-end we use a relative pose prior based on the global poses obtained from the relocalization module (Sec. V). This prior serves as initialization for the two-frame direct image alignment and replaces the motion model analogue. In addition, we construct a factor graph corresponding to the coarse-to-fine pose refinement and introduce the prior based on the relocalization poses as a factor between a reference keyframe and the current frame. If the pose prior is unavailable due to an unsuccessful relocalization attempt, the front-end is initialized according to a constant motion model, as described in [7].
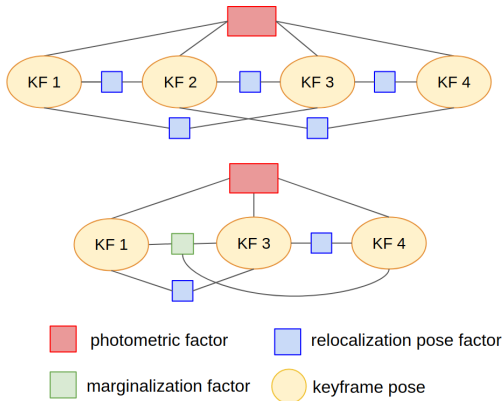
Fig. 2: Example of a factor graph with 4 keyframes in the back-end optimization. To emphasize our contribution, some variables such as observed points are not shown (see Fig. 5 in [7]). Each relocalization factor represents a relative relocalization pose between corresponding keyframes. When a keyframe is marginalized (bottom), residual energy after the Schur complement is kept as a factor (green).

2) Pose Prior for Bundle Adjustment: Keyframe poses optimized in the bundle adjustment are defined with respect to a common local coordinate frame. Therefore, one could think of lifting this common coordinate frame to a global frame based on the information obtained from relocalization and performing optimization of the global poses directly in the bundle adjustment. However, due to the marginalization of keyframes, this leads to numerical instabilities, especially in situations when relocalization poses are sparse or not available for the first frame. Hence, similar to the coarse tracker prior, we utilize relative pose priors between the keyframes respectively. We can derive a factor graph as shown in Fig. 2, where the red boxes refer to the photometric factors defined in Eq. (1) and the green boxes refer to the marginalization factors. Relocalization factors (blue boxes) are imposed in the form of priors $\widehat{\mathbf{T}}_i^j$ on the relative pose $\mathbf{T}_i^j \in \mathrm{SE}(3)$ between keyframes i and j according to Eq. (2).

$$E_{\text{pose}} = \sum_{i \in \mathcal{F}} \sum_{\substack{j \in \mathcal{R}_i \\ j < i}} \mathrm{Log}(\widehat{\mathbf{T}}_j^i \mathbf{T}_i^j)^T \mathbf{\Sigma}^{-1} \mathrm{Log}(\widehat{\mathbf{T}}_j^i \mathbf{T}_i^j) \quad (2)$$

Here $\mathcal{F}$ is a set of all keyframes and $\mathcal{R}_i$ is a subset of $\mathcal{F}$, which includes keyframes that have a relocalization pose. In our work we limit $|\mathcal{R}_i| \leq 2$. When selecting keyframes for $\mathcal{R}_i$, the priority is given to the later ones, since the oldest keyframes can be shortly scheduled for marginalization. The inverse of a covariance matrix $\mathbf{\Sigma}^{-1} \in \mathbb{R}^{6 \times 6}$ is modeled as a constant diagonal matrix and $\mathrm{Log}(\cdot)$ is a mapping from an element of the Lie group $\mathrm{SE}(3)$ to its twist coordinates in $\mathfrak{se}(3)$.

Combining photometric and relocalization factors, the total objective function becomes

$$E_{\text{total}} = E_{\text{photo}} + w E_{\text{pose}}, \quad (3)$$

where $w = 10^3$ is introduced to mitigate a large photometric error. E_{photo} and E_{pose} are defined as in Eq. (1) and Eq. (2)

respectively. The minimization of E_{total} is performed in a Gauss-Newton optimization scheme.

B. Feature Tracking

While photometric formulations show superior performance with respect to VO, they struggle in tasks like loop closure and relocalization, since in these cases a good initialization and photometric consistency cannot be guaranteed. To be able to solve these problems, we follow the idea of LDSO [6], which replaces a subset of the tracked and optimized points by keypoints with associated local descriptors. Since keypoints are tightly integrated into the photometric bundle adjustment, their accurate depth is estimated using an entire optimization window. While LDSO limits the use to handcrafted ORB features [9], we keep our pipeline more general, which enables integration of any local keypoint descriptors, including learned ones.

The tracked features now can be used to solve tasks like loop closure to generate globally consistent maps or to perform relocalization against a pre-build map (Sec. V).

V. RELOCALIZATION

Relocalization is carried out in a two-step approach. Firstly, we find potential candidates in the map database using Bag-of-Words (BoW) image retrieval (Sec. V-A). Secondly, a relative pose between a current frame and its map-based reference is estimated from feature correspondences and a global relocalization pose is computed (Sec. V-B).

A. Bag-of-Words Image Retrieval

After the system has received a new image, it extracts local 2D features and converts them to a global descriptor using a BoW database.[1] Since such a representation does not preserve the order of features in the image, it removes the spatial information of the feature layout and offers only a limited description capability. To circumvent this problem, we follow the *pyramid matching* method proposed in [28]. In particular, we switch to a multi-level representation of an image, which can be intuitively viewed as placing a grid of increasingly coarser resolution and aggregating the features in each grid cell for local histogram computations. We refer to Eq. (3) of [29] for further details of the underlying approach.

To limit the number of images considered for the similarity measure computation, we take advantage of the sequential nature of our queries and assume that the correct tracking references lie spatially close for consecutive frames.

B. Pose Refinement

We select the top three retrieval candidates from a pre-built map and proceed to feature matching. False correspondences are pruned using Lowe's ratio test [16] with threshold $\tau = 0.85$. Having 3D - 2D correspondences between a reference map frame and a current frame we can estimate 6DoF relative transformation using a Perspective-n-Points (PnP) algorithm in a RANSAC scheme [30] and refine it by minimizing a

---

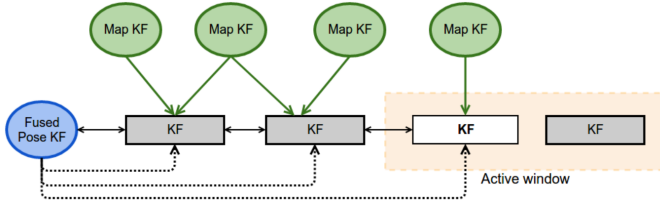[1]We use fbow, a fast version of DBoW2/DBoW3 libraries [27].

Fig. 3: Example of a fusion pose graph. Circular components represent fixed variables. Solid arrows refer to imposed constraints on the optimized variables, whereas dotted arrows represent their initialization. The direction of arrows depicts relative transformation between corresponding coordinate systems. A white rectangle denotes a keyframe that is scheduled for marginalization.

geometric projection error. The final global pose is computed by concatenating the respective relative transformation to the global pose of a map candidate that has the biggest number of feature correspondences.

VI. FUSION

In addition to the integration of relocalization poses into direct image alignment and bundle adjustment, we propose a local pose graph to fuse odometry and relocalization estimations online. Since our relocalization module computes relative poses with respect to global map poses, they are suitable as pair-wise pose observations in a traditional pose graph framework. To avoid inconsistencies caused by updates in the active window, we base our pose graph on marginalized keyframes.

The main objective of the local pose graph optimization lies in the estimation of a fused pose $\mathbf{F}_m \in \mathrm{Sim}(3)$ for a keyframe m that has been scheduled for marginalization. To build the graph we consider only keyframes that appear earlier in the sequence and have a relocalization pose. After all keyframes are chosen, pose values are initialized based on the oldest keyframe, which has already received a fused pose. Specifically, the initialization of estimated fused pose $\mathbf{F}_j$ of a keyframe j is achieved by concatenating a relative keyframe pose $\mathbf{T}_i^j$ to a fused pose $\mathbf{F}_i$ of a reference keyframe i, i.e. $\mathbf{F}_j := \mathbf{T}_i^j \mathbf{F}_i$. An example of the proposed pose graph can be seen in Fig. 3.

We distinguish two types of constraints, namely odometry-based $e_{i,j}$ and map-based $l_{i,k}$, which are defined in Eq. (4) and Eq. (5) respectively. In Eq. (5) $\mathbf{M}$ denotes a map trajectory and $\widehat{\mathbf{T}}$ corresponds to global relocalization poses.

$$e_{i,j} := \mathrm{Log}(\mathbf{T}_j^i \mathbf{F}_i^j) \tag{4}$$

$$l_{i,k} := \mathrm{Log}((\widehat{\mathbf{T}}_i \mathbf{M}_k^{-1})^{-1} \mathbf{F}_i \mathbf{M}_k^{-1}) \tag{5}$$

In Eqs. (4) and (5), $\mathrm{Log}(\cdot)$ defines the mapping from an element of the Lie group $\mathrm{Sim}(3)$ to its tangent space coordinates in $\mathfrak{sim}(3)$. The total energy, which is minimized in the local pose graph with N keyframes, is represented by Eq. (6):

$$E_{\mathrm{fusion}} = E_{\mathrm{vo}} + w E_{\mathrm{map}} \tag{6}$$
$$= \sum_{i,j \in \mathcal{F}_m} e_{i,j}^T \mathbf{\Sigma}^{-1} e_{i,j} + w \cdot \sum_{i \in \mathcal{F}_m} \sum_{k \in \mathcal{L}_i} l_{i,k}^T \mathbf{\Lambda}^{-1} l_{i,k},$$

where $\mathcal{F}_m$ is a set of selected keyframes together with the keyframe m, $\mathcal{L}_i$ is a set of tracking references for the keyframe i. Lastly, $\mathbf{\Sigma}^{-1}, \mathbf{\Lambda}^{-1} \in \mathbb{R}^{7 \times 7}$ are inverses of covariance matrices, which are modeled as constant diagonal matrices. Since the relocalization poses are computed using the PnP algorithm and 3D-2D feature correspondences (Sec. V), an odometry scale is not recovered. Thus, we set a corresponding entry in the covariance matrix $\mathbf{\Lambda}$ to a large number. A weighting factor $w = 10^2$ is chosen empirically.

In our implementation, we take advantage of the possibility of having several relocalization references per keyframe and impose at most two measurement constraints from the map. For optimizations we fix all map poses together with the reference keyframe. Our pose graph optimization is implemented based on g2o [31].

VII. EXPERIMENTS

We choose two datasets to evaluate our method, namely the 4Seasons Dataset [32] and the Oxford RobotCar Dataset [33]. 4Seasons is a novel cross-season and multi-weather outdoor dataset created by traversing nine different environments multiple times. It provides accurate ground truth 6DoF camera poses with up-to centimeter precision. For our evaluations, we select one urban environment and use the sequences corresponding to six different traversals, which were captured in March and April of 2020. Since the sequences capture minor seasonal changes, we use them as a relatively less challenging setting. Oxford RobotCar is a large-scale dataset which is created by traversing a single route in Oxford for over one year. It thus contains significantly different scene layouts, weather and seasonal conditions. For a more challenging setting, we choose 3 sequences: *2014-11-18-13-20* (cloudy), *2014-12-09-13-21* (overcast) and *2015-08-12-15-04* (sunny) and use the provided Real-time Kinematic (RTK) poses [34] as ground truth.

A. Integrating Pose Prior to Visual Odometry

To verify the benefits of integrating pose priors based on the relocalization module (Sec. IV-A) into the VO system of DSO, we conduct thorough experiments on the chosen datasets. For each dataset we create sequence pairs, such that one sequence from every pair is used for running VO, whereas the other is deployed for generating the map. Three settings are evaluated for each sequence pair, namely "no prior" (i.e. conventional VO), "prior in the front-end tracking" and "prior in both the front-end tracking and the back-end BA". In addition, we evaluate the influence of integrating different feature types into the direct method, namely a handcrafted feature, ORB [9], and three learned features, SuperPoint [25], ASLFeat [26] and R2D2 [24]. The relative pose error (RPE) [35] is adopted for quantification. As pointed out by [35], rotational errors appear as translational errors when a camera moves, we therefore only consider the translational error in meters. The relative errors are computed by using an interval of seven keyframes.

The results on the 4Seasons sequences are shown in Table I, where the rows are grouped and arranged according

| Configuration | Odometry / Map | no prior / prior in front-end / prior in front- and back-end | | | |
		ORB	SuperPoint	ASLFeat	R2D2
same sequence	03-24_17-36-22 / 03-24_17-36-22	0.31 / 0.20 / **0.11**	0.36 / **0.09** / **0.09**	**0.11** / 0.16 / 0.15	1.40 / 0.18 / **0.17**
shadows / shadows	03-24_17-36-22 / 03-24_17-45-37	0.39 / 0.40 / **0.19**	0.36 / 0.13 / **0.09**	**0.11** / 0.19 / 0.15	1.61 / 0.20 / **0.18**
sunny / sunny	04-07_10-35-45 / 04-07_10-20-32	0.42 / 0.23 / **0.19**	0.48 / 0.32 / **0.17**	0.49 / 0.24 / **0.15**	1.22 / 0.47 / **0.42**
sunny / shadows	04-07_10-35-45 / 03-24_17-36-22	0.39 / **0.25** / 0.59	0.40 / 0.32 / **0.26**	0.67 / 0.41 / **0.26**	1.46 / **0.71** / 0.86
shadows / overcast	03-24_17-36-22 / 03-03_11-52-19	0.59 / 0.39 / **0.37**	0.41 / 0.15 / **0.13**	**0.15** / 0.35 / 0.29	1.35 / 0.65 / **0.53**
sunny / foliage	04-07_10-35-45 / 04-23_19-37-00	0.40 / **0.35** / 0.64	0.40 / **0.30** / 0.37	0.69 / **0.50** / 0.54	1.45 / **1.34** / 1.44

TABLE I: Relative Pose Error (RPE) on 4Seasons sequences. Each column shows the results of integrating different features into the direct method. The values are expressed in meters and computed with an interval of seven keyframes. The best results are shown in bold.

| Configuration | Odometry / Map | no prior / prior in front-end / prior in front- and back-end | | | |
		ORB	SuperPoint	ASLFeat	R2D2
same sequence	2014-12-09-13-21-02 / 2014-12-09-13-21-02	0.11 / **0.10** / **0.10**	0.13 / 0.11 / **0.10**	0.89 / 0.26 / **0.15**	0.29 / **0.10** / 0.11
cloudy / overcast	2014-11-18-13-20-12 / 2014-12-09-13-21-02	0.27 / **0.22** / 0.23	0.38 / 0.24 / **0.15**	0.96 / 0.23 / **0.16**	0.74 / 0.17 / **0.16**
cloudy / sunny	2014-11-18-13-20-12 / 2015-08-12-15-04-18	**0.28** / 0.32 / 0.35	0.35 / 0.20 / **0.16**	1.08 / 0.32 / **0.17**	0.73 / 0.58 / **0.49**
overcast / cloudy	2014-12-09-13-21-02 / 2014-11-18-13-20-12	0.12 / **0.10** / 0.11	**0.12** / 0.14 / 0.17	0.83 / 0.23 / **0.15**	0.25 / **0.15** / 0.17
overcast / sunny	2014-12-09-13-21-02 / 2015-08-12-15-04-18	**0.11** / 0.12 / 0.13	**0.11** / 0.14 / 0.16	0.84 / 0.23 / **0.13**	0.24 / **0.16** / 0.23
sunny / cloudy	2015-08-12-15-04-18 / 2014-11-18-13-20-12	**0.12** / 0.15 / 0.22	**0.11** / 0.12 / 0.13	0.29 / 0.15 / **0.12**	0.42 / **0.29** / 0.37
sunny / overcast	2015-08-12-15-04-18 / 2014-12-09-13-21-02	**0.12** / 0.15 / 0.13	**0.12** / 0.14 / 0.15	0.27 / 0.20 / **0.15**	0.38 / 0.18 / **0.14**

TABLE II: Relative Pose Error (RPE) on Oxford RobotCar sequences. Each column shows the results of integrating different features into the direct method. The values are expressed in meters and computed with an interval of seven keyframes. The best results are shown in bold.

to increasing difficulties. Note that the first row corresponds to the case of using the same sequence for the map and VO, which is idealistic and is shown as reference. As it can be seen from the table, the pose priors based on the relocalization poses generally improve camera tracking. Some notable exceptions appear with ASLFeat for the sequences with shadows, where the relocalization accuracy is not sufficient to boost pure visual odometry estimates.

The results on Oxford RobotCar are presented in Table II. For the selected pair sequences the corresponding images from the map and VO recording often look significantly different. Therefore, the performance of matching ORB and SuperPoint features starts to degrade, and the integration of pose priors does not result in the improvement when compared to pure VO. It should be noted, though, that despite underperforming feature matching, our integration maintains the system stability and does not significantly worsen the VO performance. On the other hand, in these more challenging conditions, relocalization based on more advanced features like ASLFeat and R2D2 helps to improve over pure VO, as shown in the last two columns.

B. Map-Based Relocalization and Fusion with VO

In this section, we verify the quality of the global relocalization poses and the benefit of fusing them with the VO output. As explained in Section VI, our fusion method can estimate global poses defined in the reference coordinate system of the map. This makes it possible to evaluate the global pose errors. In all the following experiments, the absolute trajectory error (ATE) [35] is used.

On the 4Seasons dataset we select three sequence pairs with increasingly challenging configurations on weather and seasonal conditions, namely "shadows / shadows", "shadows / overcast" and "sunny / foliage". The two features that work dedicatedly on grayscale images, namely ORB

and SuperPoint, are evaluated. The cumulative error plots together with some example images from the odometry and the map sequences are shown in Fig. 4. It is apparent that fusing the relocalization poses with the VO results consistently improves pose accuracy. It is worth noting that the relocalization curves often saturate to values less than 100%, which means we do not get relocalization poses for all keyframes. Yet our fusion unquestionably boosts the performances in those cases. Due to the significant differences caused by seasonal change, relocalization based on ORB features is unsuccessful for the majority of keyframes in the configuration of "sunny / foliage". Therefore, fusion estimates are not globally accurate in this case.

We further verify our relocalization and fusion on the Oxford RobotCar dataset, using the same sequence pairs as in the previous section. All the four selected features are tested and the cumulative absolute errors are shown in Fig. 5. Despite the more challenging configurations compared to the 4Seasons experiments, our fusion consistently improves the performances over relocalization for all the tested features.

C. Runtime

Table III presents a timing assessment of our system. The values are collected on a machine with Intel Core i7-8700K CPU, 32 GB RAM. We demonstrate results for ORB and SuperPoint features to account for the differences in their extraction and description.

As it can be seen from the table, relocalization based on ORB features is fast, which allows tracking to be performed in real-time. Inference of SuperPoint features remains a bottleneck, which can be mitigated by porting inference to GPU and incorporating further optimization techniques. To adhere to spatial BoW image retrieval, multi-level histograms can be computed in parallel. BA and fusion run at a keyframe rate and, therefore, are not limiting the real-time performance.

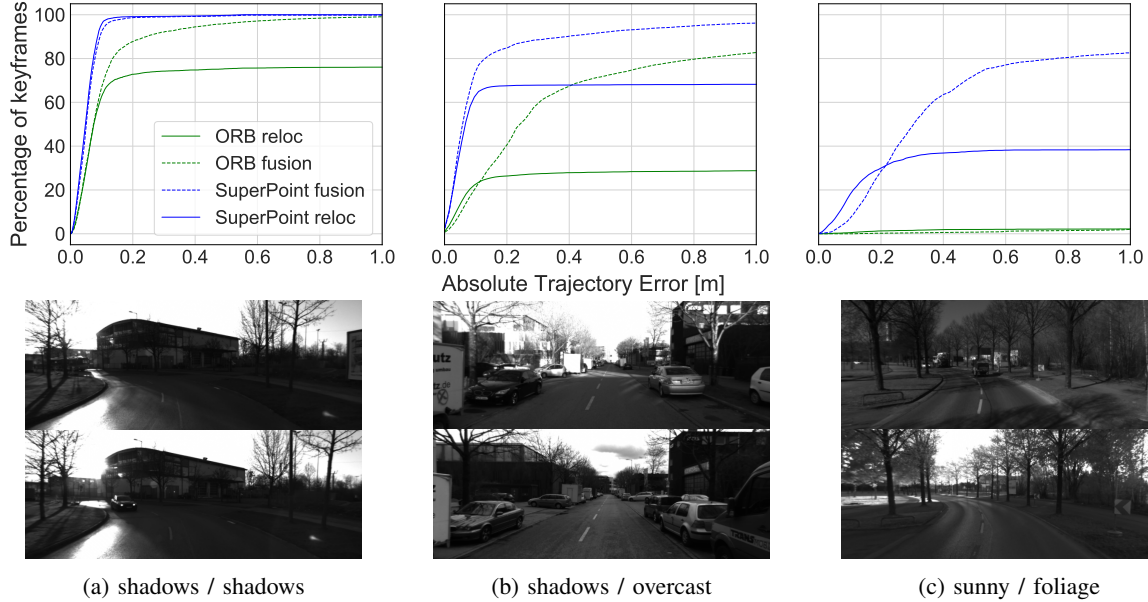| (a) shadows / shadows | (b) shadows / overcast | (c) sunny / foliage |

Fig. 4: Cumulative Absolute Trajectory Error on 4Seasons sequences. Fusing relocalization poses with VO in a pose graph consistently improves the absolute pose accuracy. Note that ORB does not perform well for "sunny / foliage" due to the low relocalization success rate caused by significant appearance changes.

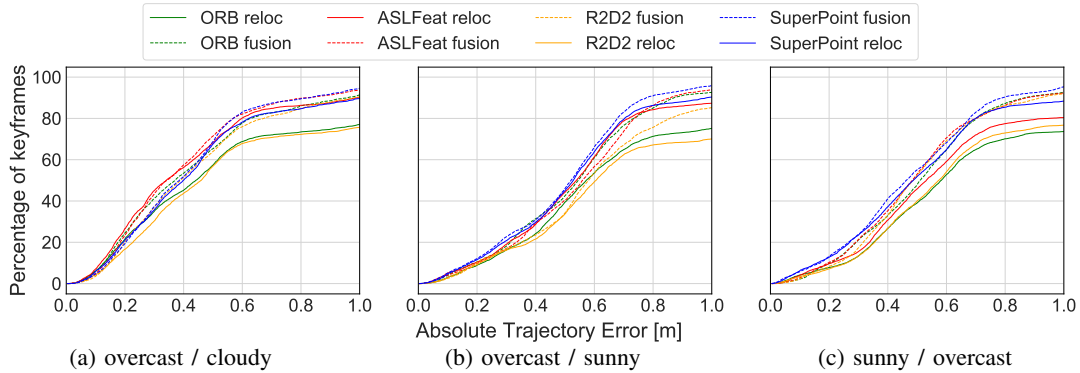| (a) overcast / cloudy | (b) overcast / sunny | (c) sunny / overcast |

Fig. 5: Cumulative Absolute Trajectory Error on Oxford RobotCar sequences. Fusing the relocalization poses with VO in a pose graph consistently improves the performances.

Task		Rate	Mean ± std [ms]	
			ORB	SuperPoint
Reloc	Feature Extraction	F	5.63 ± 1.04	220.93 ± 5.70
	IR BoW	F	2.85 ± 0.27	2.26 ± 0.33
	Spatial BoW		7.08 ± 2.79	8.50 ± 4.51
	Pose Estimation	F	8.93 ± 7.27	9.60 ± 4.16
	Coarse Tracker	F	2.66 ± 13.06	
	BA + Marginalization	KF	60.60 ± 11.93	
	Fusion	KF	3.54 ± 1.11	

TABLE III: Runtime evaluation in milliseconds on the 4Seasons dataset. Relocalization is performed on the shadows / shadows odometry-map setting. Tasks run at the frame (F) or the keyframe-rate (KF) (5 - 10 keyframes per second [7]).

VIII. CONCLUSION

In this paper we present a complete framework which combines direct VO and feature-based relocalization in an online and tightly-coupled fashion. We extensively evaluate our approach on two multi-weather datasets. Our experiments show that by integrating pose priors obtained from relocalization into both the front-end tracking and the back-end optimization of a direct VO method, we can significantly improve the tracking accuracy. We also show that the proposed fusion module is able to estimate globally accurate poses, even when relocalization is not successful for every frame. Furthermore, using our pipeline we leverage the strengths and uncover some of the weaknesses of different feature types. We hope that our work has revealed the power of combining direct and indirect approaches in the context of simultaneous localization and mapping (SLAM) and that it will drive further research in this direction.

REFERENCES

[1] C. Cadena, L. Carlone, H. Carrillo, Y. Latif, D. Scaramuzza, J. Neira, I. Reid, and J. J. Leonard, "Past, present, and future of simultaneous localization and mapping: Toward the robust-perception age," *IEEE Transactions on Robotics (T-RO)*, vol. 32, no. 6, pp. 1309–1332, 2016.

[2] J. Fuentes-Pacheco, J. Ruiz-Ascencio, and J. M. Rendón-Mancha, "Visual simultaneous localization and mapping: A survey," *Artificial Intelligence Review*, vol. 43, no. 1, pp. 55–81, 2015.

[3] G. Klein and D. Murray, "Parallel tracking and mapping for small AR workspaces," in *International Symposium on Mixed and Augmented Reality (ISMAR)*, pp. 225–234, 2007.

[4] R. Mur-Artal, J. M. M. Montiel, and J. D. Tardos, "ORB-SLAM: A versatile and accurate monocular SLAM system," *IEEE Transactions on Robotics (T-RO)*, vol. 31, no. 5, pp. 1147–1163, 2015.

[5] L. von Stumberg, P. Wenzel, Q. Khan, and D. Cremers, "GN-Net: The gauss-newton loss for multi-weather relocalization," *IEEE Robotics and Automation Letters (RA-L)*, vol. 5, no. 2, pp. 890–897, 2020.

[6] X. Gao, R. Wang, N. Demmel, and D. Cremers, "LDSO: Direct sparse odometry with loop closure," in *IEEE/RSJ International Conference on Intelligent Robots and Systems (IROS)*, pp. 2198–2204, 2018.

[7] J. Engel, V. Koltun, and D. Cremers, "Direct sparse odometry," *IEEE Transactions on Pattern Analysis and Machine Intelligence (TPAMI)*, vol. 40, no. 3, pp. 611–625, 2017.

[8] N. Yang, L. v. Stumberg, R. Wang, and D. Cremers, "D3VO: Deep depth, deep pose and deep uncertainty for monocular visual odometry," in *IEEE/CVF Conference on Computer Vision and Pattern Recognition (CVPR)*, pp. 1281–1292, 2020.

[9] E. Rublee, V. Rabaud, K. Konolige, and G. Bradski, "ORB: An efficient alternative to SIFT or SURF," in *IEEE International Conference on Computer Vision (ICCV)*, pp. 2564–2571, 2011.

[10] A. J. Davison, I. D. Reid, N. D. Molton, and O. Stasse, "MonoSLAM: Real-time single camera SLAM," *IEEE Transactions on Pattern Analysis and Machine Intelligence (TPAMI)*, vol. 29, no. 6, pp. 1052–1067, 2007.

[11] H. Jin, P. Favaro, and S. Soatto, "A semi-direct approach to structure from motion," *The Visual Computer*, vol. 19, no. 6, pp. 377–394, 2003.

[12] J. Engel, T. Schöps, and D. Cremers, "LSD-SLAM: Large-scale direct monocular SLAM," in *European Conference on Computer Vision (ECCV)*, pp. 834–849, 2014.

[13] S. Agarwal, Y. Furukawa, N. Snavely, I. Simon, B. Curless, S. M. Seitz, and R. Szeliski, "Building rome in a day," *Communications of the ACM*, vol. 54, no. 10, pp. 105–112, 2011.

[14] T. Sattler, B. Leibe, and L. Kobbelt, "Fast image-based localization using direct 2D-to-3D matching," in *IEEE International Conference on Computer Vision (ICCV)*, pp. 667–674, 2011.

[15] J. L. Schönberger, T. Price, T. Sattler, J.-M. Frahm, and M. Pollefeys, "A vote-and-verify strategy for fast spatial verification in image retrieval," in *Asian Conference on Computer Vision (ACCV)*, pp. 321–337, Springer, 2016.

[16] D. G. Lowe, "Distinctive image features from scale-invariant keypoints," *International Journal of Computer Vision (IJCV)*, vol. 60, no. 2, pp. 91–110, 2004.

[17] E. Rosten and T. Drummond, "Machine learning for high-speed corner detection," in *European Conference on Computer Vision (ECCV)*, pp. 430–443, 2006.

[18] M. Calonder, V. Lepetit, C. Strecha, and P. Fua, "BRIEF: Binary robust independent elementary features," in *European Conference on Computer Vision (ECCV)*, pp. 778–792, 2010.

[19] J. L. Schönberger, H. Hardmeier, T. Sattler, and M. Pollefeys, "Comparative evaluation of hand-crafted and learned local features," in *IEEE/CVF Conference on Computer Vision and Pattern Recognition (CVPR)*, pp. 1482–1491, 2017.

[20] S. Huang, M. Gong, and D. Tao, "A coarse-fine network for keypoint localization," in *IEEE International Conference on Computer Vision (ICCV)*, pp. 3028–3037, 2017.

[21] S. Suwajanakorn, N. Snavely, J. J. Tompson, and M. Norouzi, "Discovery of latent 3D keypoints via end-to-end geometric reasoning," in *Conference on Neural Information Processing Systems (NeurIPS)*, pp. 2059–2070, 2018.

[22] V. Balntas, E. Riba, D. Ponsa, and K. Mikolajczyk, "Learning local feature descriptors with triplets and shallow convolutional neural networks.," in *British Machine Vision Conference (BMVC)*, 2016.

[23] K. M. Yi, E. Trulls, V. Lepetit, and P. Fua, "LIFT: Learned invariant feature transform," in *European Conference on Computer Vision (ECCV)*, pp. 467–483, 2016.

[24] J. Revaud, C. De Souza, M. Humenberger, and P. Weinzaepfel, "R2D2: Reliable and repeatable detector and descriptor," in *Conference on Neural Information Processing Systems (NeurIPS)*, pp. 12405–12415, 2019.

[25] D. DeTone, T. Malisiewicz, and A. Rabinovich, "SuperPoint: Self-supervised interest point detection and description," in *IEEE/CVF Conference on Computer Vision and Pattern Recognition Workshops*, pp. 224–236, 2018.

[26] Z. Luo, L. Zhou, X. Bai, H. Chen, J. Zhang, Y. Yao, S. Li, T. Fang, and L. Quan, "ASLFeat: Learning local features of accurate shape and localization," in *IEEE/CVF Conference on Computer Vision and Pattern Recognition (CVPR)*, pp. 6589–6598, 2020.

[27] D. Gálvez-López and J. D. Tardós, "Bags of binary words for fast place recognition in image sequences," *IEEE Transactions on Robotics (T-RO)*, vol. 28, pp. 1188–1197, October 2012.

[28] K. Grauman and T. Darrell, "The pyramid match kernel: Discriminative classification with sets of image features," in *IEEE International Conference on Computer Vision (ICCV)*, vol. 2, pp. 1458–1465, 2005.

[29] S. Lazebnik, C. Schmid, and J. Ponce, "Beyond bags of features: Spatial pyramid matching for recognizing natural scene categories," in *IEEE/CVF Conference on Computer Vision and Pattern Recognition (CVPR)*, vol. 2, pp. 2169–2178, 2006.

[30] M. A. Fischler and R. C. Bolles, "Random sample consensus: a paradigm for model fitting with applications to image analysis and automated cartography," *Communications of the ACM*, vol. 24, no. 6, pp. 381–395, 1981.

[31] G. Grisetti, R. Kümmerle, H. Strasdat, and K. Konolige, "g2o: A general framework for (hyper) graph optimization," in *IEEE International Conference on Robotics and Automation (ICRA)*, pp. 9–13, 2011.

[32] P. Wenzel, R. Wang, N. Yang, Q. Cheng, Q. Khan, L. von Stumberg, N. Zeller, and D. Cremers, "4Seasons: A cross-season dataset for multi-weather SLAM in autonomous driving," in *German Conference on Pattern Recognition (GCPR)*, 2020.

[33] W. Maddern, G. Pascoe, C. Linegar, and P. Newman, "1 year, 1000 km: The Oxford RobotCar dataset," *International Journal of Robotics Research (IJRR)*, vol. 36, no. 1, pp. 3–15, 2017.

[34] W. Maddern, G. Pascoe, M. Gadd, D. Barnes, B. Yeomans, and P. Newman, "Real-time kinematic ground truth for the Oxford Robot-Car dataset," *arXiv preprint arXiv:2002.10152*, 2020.

[35] J. Sturm, N. Engelhard, F. Endres, W. Burgard, and D. Cremers, "A benchmark for the evaluation of RGB-D SLAM systems," in *IEEE/RSJ International Conference on Intelligent Robots and Systems (IROS)*, pp. 573–580, 2012.